Journal of Applied Polymer Science

Efficient wound odor removal by β-cyclodextrin functionalized poly (ε-caprolactone) nanofibers

Ganesh Narayanan,[1] Bryan R. Ormond,[2] Bhupender S. Gupta,[1] Alan E. Tonelli[1]

[1]Fiber and Polymer Science Program, North Carolina State University, Raleigh, North Carolina 27695-8301

[2]Textile Protection and Comfort Center (T-PACC), North Carolina State University, Raleigh, North Carolina 27695-8301

Correspondence to: A. E. Tonelli (E-mail: alan_tonelli@ncsu.edu)

ABSTRACT: Polymer-cyclodextrin (CD) composite nanofibers, by virtue of the hollow cavities and abundant hydroxyl groups present in CDs, have tremendous potential in a variety of biomedical applications. However, in most cases, especially in aliphatic polyesters, polymer chains thread readily into CD cavities, therefore its potential has not yet been fully realized. Herein, we report the formation of poly(ε-caprolactone) (PCL)/β-CD functional nanofibers by electrospinning their mixture from chloroform/*N*,*N*-dimethylformamide (60 : 40). The fiber diameters of the neat PCL and β-CD functionalized fibers were measured from the images obtained from a scanning electron microscope and were found to be about 500 nm. The efficiency of wound odor absorbance by these composite fibers was studied using a simulated wound odor solution, consisting of butyric and propionic acids in ethanol. Immersion tests indicated that even under less than ideal test conditions, the nanofibers containing β-CDs were very efficient in masking the odor. The odor masking capability of the β-CD functionalized PCL nanofibers were further confirmed by thermogravimetric analyses and GC observations, with the former method showing unique degradation patterns. The PCL/β-CD nanocomposites, by virtue of having their β-CD cavities free and unthreaded by PCL, could potentially be an ideal substrate for removing wound odors through formation of inclusion compounds with odorants, while providing an ideal environment for the wound to heal. These results suggest tailoring polymer-CD nanostructures for specific applications in wound odor absorbance, surface grafting of chemical moieties, and vehicles for drug delivery, as examples. © 2015 Wiley Periodicals, Inc. J. Appl. Polym. Sci. **2015**, *132*, 42782.

KEYWORDS: electrospinning; fibers; functionalization of polymers; properties and characterization; surfaces and interfaces

Received 11 June 2015; accepted 24 July 2015

DOI: 10.1002/app.42782

INTRODUCTION

Although the electrospinning process for producing nanofibers in the range of 5–500 nm has been known for about a century, the last two decades has seen an explosion in utilizing this process to make nanofibers for innovative applications in filtration, wound dressing/healing, scaffolds, and so forth.[1–5] The advantage of using electrospinning, apart from being a simple method for fabrication, is its ability to form nanosized fibers in various shapes, such as porous, hollow, and core-sheath structures.[6–9] Two techniques commonly utilized to prepare porous nanofibers include: choosing solvents with high vapor pressure, which evaporate readily during electrospinning, resulting in the formation of porous nanofibers, or deliberately adding salt to the polymer solution and leach the latter out once the fibers are dried.[10,11] Because of their enhanced surface to volume ratios, compared with the regular solid cylindrical nanofibers,the porous and hollow fibers are also highly desired for enhanced filtration applications.

Wound healing is a complicated process, during which the body initially forms a fibrin plug to establish homeostasis, and is aided by the secretion of several growth factors. The process of wound healing is complete when new extra cellular matrix (ECM) is formed, replacing the old ECM.[12–14] The wound healing process is, however, hindered in some patients, especially those suffering from diabetes or metastasized cancer, resulting in chronic wounds that are normally nonhealing.[15] Other factors that affect wound healing include: the pH of wounded tissue, oxygen permeability, moisture of the wound environment, and nonadherence of the dressing to the wound.[16–19]

When the wound does not heal properly and quickly, foul odors emanate from the exudates. The malodor from the wound is mainly because of the liberation of volatile fatty acids such as acetic, butyric, propionic, and valeric acids, and amines, such as putrescine and cadaverine, which are produced by various bacteria from serum protein.[20] The composition of wounds, however, have been found

Additional Supporting Information may be found in the online version of this article.

to vary depending on the type/location of the wound, age, and general health of the patient, and many other factors.

Commonly used wound dressings include hydro-fibers, hydrocolloids, hydrogels, foams and films.[21–24]Apart from topical agents such as metronidazole, activated charcoal based dressings are widely used to absorb the malodor emanating from chronic non-healing wounds. These dressings, however, lose their efficiency when they come in contact with exudates with high moisture content.[25] Hence, there is a definite need for novel wound absorbent material which can absorb the volatile foul smelling compounds when in contact with moist exudates, and which simultaneously retain its structure, thereby reducing the necessity for frequent dressing changes.

Cyclodextrins (CDs) belong to a group of cyclic α-1,4-linked oligosaccharides. Most widely used CDs are α-, β-, and γ-CD, which have 6, 7, and 8 glucopyranose units respectively. CDs have a truncated conical shape with a hollow interior that enables CDs to form inclusion complexes (ICs) with guest molecules. The size of interior cavities depends on the number of glucose units and are found to have diameters of 5.7, 7.8, and 9.5Å, for α-, β-, and ɤ-CDs, respectively.[26,27] Depending on the nature of guest molecules, cyclodextrin-inclusion complex (CD-IC) formation results in either of two crystalline forms: cage and columnar structures.[28] The cage structures are observed when ICs are formed with small molecules as guests, and columnar structures are observed when long molecule like polymers or other small molecules, such as long chain carboxylic acids like valeric acid, are used as guests.[29–31]

CDs are used in a variety of applications including, pharmaceutical, food, packaging, cosmetics, and in physically nanostructuring polymers.[32–34] A CD containing hydrocolloid dressing has been marketed under the trade name exuderm® odorshield® (Medline), and has been reported to be more effective than activated charcoal based dressings.[25] However, being a hydrocolloid dressing, it requires frequent dressing changes, resulting in trauma to the injury site; while a slightly hydrophobic material in fibrous form would require less frequent dressing changes.

Recently, there has been growing interest in using cyclodextrin functionalized nanofibers for filtration, drug delivery, and food packaging[35–39] In a previous report, we reported the successful formation of functional PCL nanofibers containing α- and γ-CDs.[40] It was observed that, α-CD, and to some extent γ-CD, had formed inclusion complexes (ICs) with PCL; therefore its inclusion complex forming capability with small molecule guests are expected to be somewhat diminished, which was evident with the molecular encapsulation study of phenolphthalein as a guest molecule. Although α- and γ-CD have been known to form ICs with PCL, with, respectively, single and pairs of side-by-side chains in each channel,[41–43] β-CDs, however, are not expected to form an IC with PCL because of the size mismatch between the two.[44,45] This could then provide an opportunity for free uncomplexed β-CDs to absorb small molecule guests.

In this report, we describe the formation and characterization of functionalized PCL/β-CD nanofibers and their subsequent capability to absorb wound odor components, such as butyric and propionic acids, as determined by X-ray photoelectron spectroscopy (XPS) and thermogravimetric analysis (TGA). As mentioned before, butyric and propionic acids are only two of the many components typically found in wound exudate, and these experiments serve only as proof of concept to compare the efficiency of absorption with respect to β-CD loadings. Also, since β-CDs are water soluble, instead of water, these tests were performed by diluting the acids in ethanol. With recent advancements, shown by Uyar and coworkers, in crosslinking the polymer-CD structures using citric acid,[46] which would prevent leeching of CDs by water, it should be possible CD functionalized nanofibers to be used for not only for filtration applications, but also biomedical applications such as wound odor removal.

MATERIALS AND METHODS

Poly (ε-caprolactone) with a molecular weight of 60,000 to 80,000 (M_n), chloroform (99.5%), and *N,N*-dimethyl formamide (anhydrous 99.8%), butyric and propionic acids, ethyl alcohol (99%+ purity), were obtained from Sigma-Aldrich, St. Louis, Missouri, USA. β-CD was obtained as a gift from Wacker Chemie, Michigan, USA.

Electrospinning Solution Preparation

PCL/β-CD solutions were prepared in accordance with our previous work, where PCL/α-CD and PCL/γ-CD solutions were prepared.[40] Briefly, PCL and β-CD solutions were prepared by dissolving them separately in chloroform and DMF, respectively, at 70°C on a hot plate under stirring. The two solutions were then mixed together to form combined PCL/β-CD solution/suspension in chloroform/DMF. Once the dissolution is complete, the solutions were allowed to stir overnight at room temperature. PCL concentration was set at 12% (*w/v*), and CD concentration was varied from 0%–60%, with respect to the weight of PCL.

PCL/β-CD Composite Preparation

In our previous report,[40] we studied in detail the effect of PCL concentration and % α- and γ-CD loadings on viscosity, surface tension,conductivity, and the resulting nanofiber morphology. Since, β-CD is very similar, the effects of % loadings of β-CD on the viscosity or surface tension or conductivity were not conducted for this report. We reported that with the addition of CDs, there was no significant difference in the surface tension or conductivity values, and hence this was assumed to be the same in this case, as well. Further, we had observed 12% concentration of PCL to be optimal, and up to 40% CD loadings were possible with no significant agglomeration. In this context, PCL/β-CD solutions were electrospun with only slight modification from our previous reported protocol.

Briefly, polymer solutions were held in a 10 cc syringe, to which a blunted needle (22G) was attached. A high precision pump (New Era Pump Systems, Farmingdale, NY) was used to deliver fluid at a rate of 1 mL/hr. In our previous report, we had used a feed rate of 0.5 mL/hr, which was observed to be unsuitable for PCL/β-CD solutions. Due to the precipitation of β-CD, needles clogged frequently, but when spun at a rate of 1 mL/ hr, continuous spinning was possible with no clogging. The potential difference (15 kV) between the polymer solution and the collector was applied by a Gamma High Voltage Research instrument (Ormond Beach, FL). A rotating roller (1.5 inches in diameter), made of stainless steel

was used as collector. The latter was rotated at 280 rpm (linear velocity of 28 m/min), and was placed at 30 cm from the tip of the needle. To remove residual solvent (DMF), once the experiment was completed, the obtained nanomats were degassed by placing them in a vacuum chamber for 1 week, before any further testing.

PCL/β-CD Nanowebs Characterization

The electrospun mats were characterized using Fourier Transform Infrared Spectroscopy (FTIR), thermogravimetric analyses (TGA), scanning electron microscopy (SEM), gas chromatography, X-ray photoelectron spectroscopy, and wide-angle X-ray diffraction (WAXD). Infrared spectral studies were conducted using a Nicolet 470 FTIR infrared spectrophotometer in the frequency range of 4000-400 cm^{-1} with a resolution of 4 cm^{-1}. Sixty-four scans were collected for each sample. The degradation patterns of the nanowebs were observed through a TA Q500 v6.7 thermogravimetric analyzer. The samples were heated from 25°C to 500°C at the rate of 20°C under nitrogen atmosphere. The data were analyzed using TA universal analysis software. The fiber morphology was studied with a Phenom world G1 model scanning electron microscope at an acceleration voltage of 10 kV. Since the samples are nonconductive, prior to SEM analyses, they were coated with gold, using a Polaron SC7620 Mini Sputter Coater (Quorum technologies). SEM images were obtained at various resolutions, and the fiber diameters were calculated using ImageJ software. Diameters of a minimum of 100 fibers were measured, and their average fiber diameters are reported.

WAXD analyses were performed on electrospun neat PCL, PCL/β-CD nanocomposites, and powdered samples of β-CD using a Philips type-F X-ray diffractometer with a Ni-filtered Cu Kα radiation source ($\lambda = 1.5$ Å). While electrospun webs were attached to the metal stub and taped using a double sided carbon tape, a uniform surface of β-CD powder was obtained by placing it in a glass cup and patting it gently. The applied voltage and current used were 35 kV and 25 mA, respectively, and the diffraction intensities were measured from 2θ of 5° to 40°, at the rate of 0.05°/second.

X-ray photoelectron spectroscopy experiments were performed using a SPECS Flex mode XPS instrument with an Mg Kα anode monochromator (1254 eV) as a source, with X-ray energy of 10 kV, and a hemispherical analyzer PHOIBIS 150. The takeoff angle was normal to the surface with an X-ray incidence angle of ~30°, and an X-ray source to analyzer angle of ~60°. Base pressure in the analysis chamber was in the 10^{-10} mbar range. Energy calibration was established by referencing to adventitious carbon (C1s line at 285.0 eV binding energy). Once broad spectra were collected, and the elemental composition established, in-depth higher resolution spectra were obtained for speciation analyses (C1s and O1s, in this case). CASA XPS software was used for data analyses.

The hydrophilicity of the electrospun mats was measured at room temperature using a Ramé-Hart goniometer equipped with a high-definition camera. Water contact angle measurements (WCA) were conducted on small samples (1 cm x 5 cm) which were held firmly on the stage by double-sided tape, using DI water with a bulk resistivity of 14 MΩ. Water droplets of ~12 μL were applied, and changes in droplet morphology were captured digitally, immediately and after 30 s of contact. A total of five experiments were performed on each sample group. Water contact values were then obtained by processing the images through the drop-snake ImageJ plugin developed by Stalder and coworkers.[47] In this method, image files in the form of BMP were opened using ImageJ with the drop-snake plugin. Boundary conditions were then established manually, and the software calculated the contact angle automatically on either side of the droplet (right and left sides). For simplicity, values on the right side alone were considered. Statistical comparisons (*t*-test) were made using Minitab software, version 15.

Wound Odor Absorption Test

Simulated wound fluid was prepared by dissolving 0.58 grams each of butyric and propionic acids in 55 mLof ethanol to prepare a 2.1% solution. The prepared wound odor solution was further separated into nine equal parts, and placed in separate vials. Small samples of nanoweb weighing about 0.2 g were cut from the mat and placed in the vials. At designated time intervals, the samples were taken out, and dried in a vacuum oven to remove any surface adsorbed fatty acids. The samples were then analyzed using XPS to determine the presence and concentration of butyric and propionic acid and corresponding changes in the composition before and after the absorption tests. The degradation patterns of samples before and after immersion were observed by TGA.

RESULTS

In our previous report, we had observed that critical entanglement begins at around 10%–12% for PCL in the chloroform/dimethyl formamide (60 : 40) mixture. Also we had observed that at 14% PCL concentration, both neat as well as CD functionalized PCL nanofibers produced larger fiber diameters, which was because of the viscosity effect. However, when the PCL solute concentration was lowered to 12%, higher loading of CD was possible; although there was a slight increase in fiber diameters. Since β-CD is very similar to α- and γ-CDs, significant differences in solution properties, such as viscosity, surface tensions, and conductivity, are not expected, when compared with α- and γ-CD solutions. Hence the PCL concentration was set at 12%, and β-CD loading varied from 0–50%. Interestingly, when β-CD is used, unlike α- and γ-CDs, CD loading up to 50% is possible.

The composition of PCL/β-CD solutions and the key fiber statistics obtained from the resultant electrospun nanofibers are listed in Table I. Representative scanning electron microscope images of electrospun neat PCL and β-CD functionalized PCL nanofibers (all at the same magnification and length scale) containing different amounts of β-CD, and the fiber diameter distributions are shown in Figures 1 and 2, respectively. The diameters of the β-CD functionalized nanofibers are somewhat greater compared with that of the neat PCL mats. Moreover, the fiber diameter distribution indicates that β-CD agglomeration possibly took place, resulting in statistical outliers increasing with the β-CD loading. This is likely because of the

Table I. The Composition of PCL/β-CD Solutions and Key Statistics of Resulting Electrospun PCL and PCL/β-CD Nanofibers

Solution	% β-CD[a] (w/w)	Average fiber diameter (nm)	Median (nm)	First quartile(nm)	Third quartile (nm)
Neat PCL	-	400±160	370	260	470
PCL/10-β-CD	10	520±200	490	370	640
PCL/20-β-CD	20	500±220	480	340	630
PCL/30-β-CD	30	570±270	490	410	680
PCL/40-β-CD	40	560±260	500	370	660
PCL/50—β-CD	50	570±310	500	410	660

[a] % β-CD, with respect to PCL, PCL concentration used was 12% (m/v).

turbidity of the solutions, which arises from precipitation of β-CDs from the CFM/DMF solution mixture. It is important to note that β-CDs are highly insoluble in CFM, and hence should tend to precipitate.

FTIR spectroscopy was utilized to observe the vibrational bands of the individual components, i.e.,PCL and β-CD, and observe if there was any slight peak shifts which correspond to IC formation. The FTIR spectra of pure β-CD, electrospun PCL nanofibers, PCL/20% β-CD, and PCL/40% β-CD are shown in Figure3. In the FTIR spectrum of β-CD powder, characteristic peaks were observed at 1029 cm^{-1}because of the C−O bending vibration, at 1157 cm^{-1}because of C–O stretching, and a broad absorption peak at 3347 cm^{-1} because of O–H bending vibration.[48] In the FTIR spectra of electrospun PCL nanofibers, characteristic peaks were observed at 2944 cm^{-1} and 2887 cm^{-1}

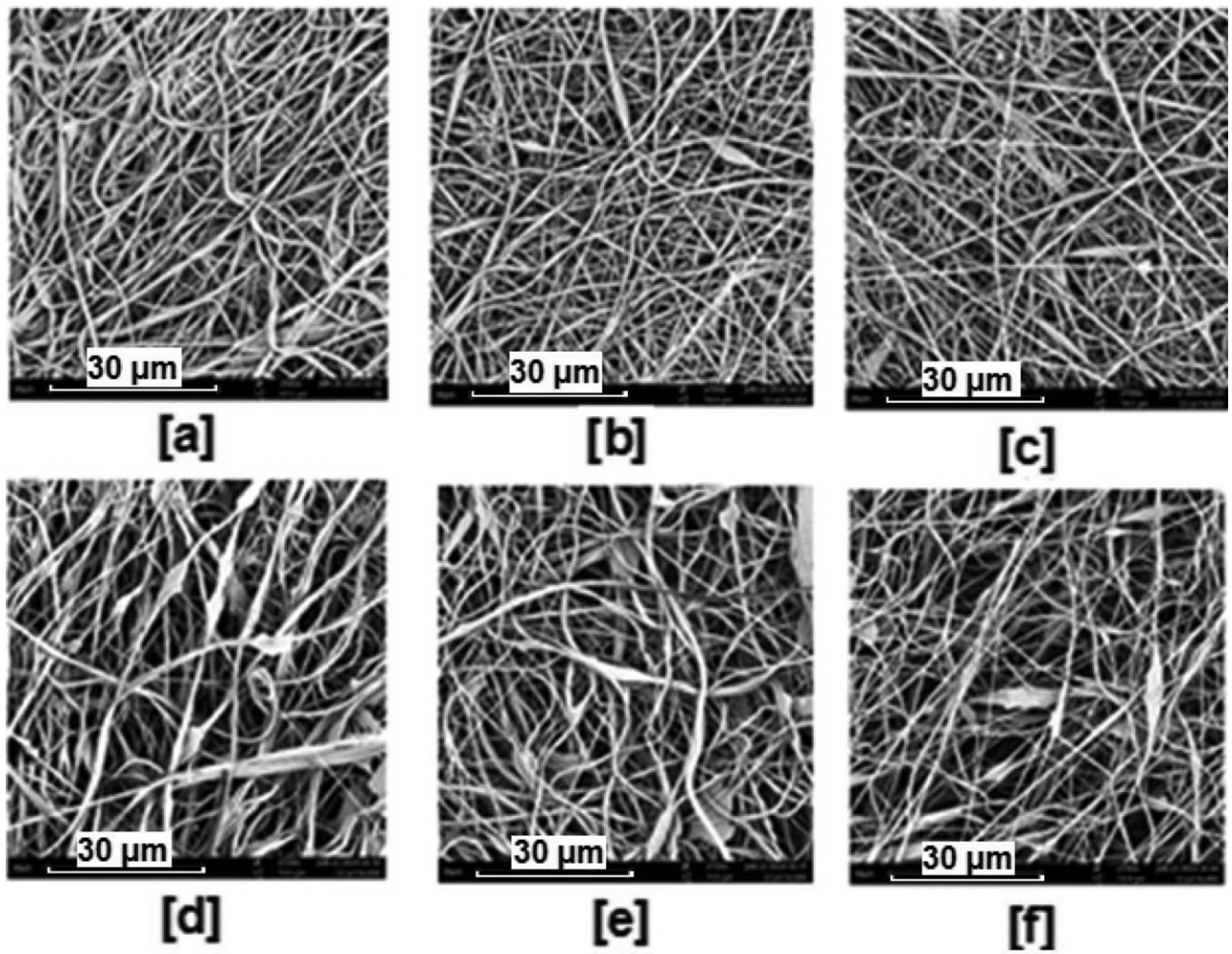

Figure 1. SEM images of electrospun nanofibers of (a) neat PCL, (b) PCL/10% β-CD, (c) PCL/20% β-CD, (d) PCL/30% β-CD, (e) PCL/40%β-CD, (f) PCL/50% β-CD.

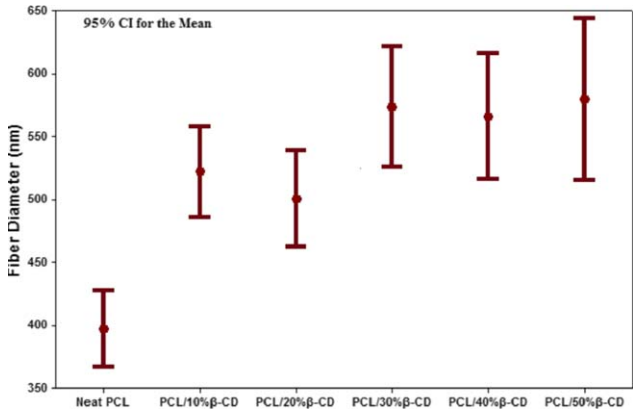

Figure 2. Fiber diameter distributions of electrospun neat PCL and PCL/β-CD nanofibers. [Color figure can be viewed in the online issue, which is available at wileyonlinelibrary.com.]

corresponding to asymmetric and symmetric CH_2 stretching. The carbonyl peak, which was predominant, was observed at 1727 cm^{-1}, and another dominant peak at 1168 cm^{-1} was observed that corresponds to symmetric C–O–C stretching. Apart from these dominant peaks, several minor peaks were observed that can be attributed to PCL. However, in the electrospun PCL/CD mats, mostly dominant peaks of PCL were visible; because of overlapping between the peaks of CDs and PCL, most of the peaks that are attributed to CDs could not be identified, except for a slight halo-like peak at 3347 cm^{-1}. Since the ATR-FTIR typically penetrates deep into the bulk, most nanoscale properties or presence of bonds on the surface typically become invisible.[49] The presence of an O–H peak at 3347 cm^{-1} and C–O stretching at 1157 cm^{-1} peak in the nanofibers only indicate the presence of both PCL as well as β-CD; however, further information about the nature of these nanofibers could not be inferred from FTIR. To investigate the surface characteristics of the nanofibers, XPS was used (discussed later). The XRD patterns of the pure β-CD, electrospun PCL, and functionalized PCL/β-CD nanofibers are shown in Figure4. XRD diffractograms of β-CD indicate a series of peaks, especially between 2θ of 17° to 34°, confirming the cage structure of native β-CD. PCL, being a semicrystalline material with orthorhombic crystal structure, exhibits two distinct peaks at 2θ= 22° and 24° that corresponds to (110) and (200) lattice structures, respectively. In the case of functionalized fibers, it is clearly evident that the characteristic peaks of PCL at $2\theta = 24°$ has broadened, and the intensity of the peak at $2\theta = 22°$ has decreased significantly and shifted slightly to the right. Also, in general, the visibility of the β-CD peaks diminished, and the absence of a crystalline peak at $2\theta = 18°–19°$, expected of ICs, indicates that PCL and β-CD have not threaded.[50]

In a physical mixture, however, no additional peaks are expected and all peaks are expected to resemble the individual components, with their intensities depending on their ratio. When any interaction occurs between components, however, a decrease in peak intensity and an increase in peak width is expected to be typically observed.[51] Although, still a hypothesis, such results observed in our functionalized samples point out that some interaction between PCL and β-CD occurred. Formation of IC, however, can be discarded, since the corresponding IC peaks were not observed. Figures 5 and 6 illustrate the TGA thermograms of neat PCL, PCL/10% β-CD, PCL/30% β-CD, and PCL/50% β-CD, obtained from 25°C to 600°C, and the magnified thermograms from 25°C to 150°C, respectively. The thermograms of PCL nanofibers indicate that the degradation starts at about 370°C, with significant weight loss observed above 400°C. In the case of functionalized PCL nanofibers, a three step degradation pattern was observed. Firstly, from about 50°C to 125°C (Figure6), dehydration of the nanowebs took place, which indicates the presence of β-CDs.[52] This is followed by degradation of β-CDs from 320°C to about 370°C. Beyond this, the degradation of PCL was observed. It is quite obvious that, with the addition of β-CDs, improvement in thermal stability, typically found for ICs, was not

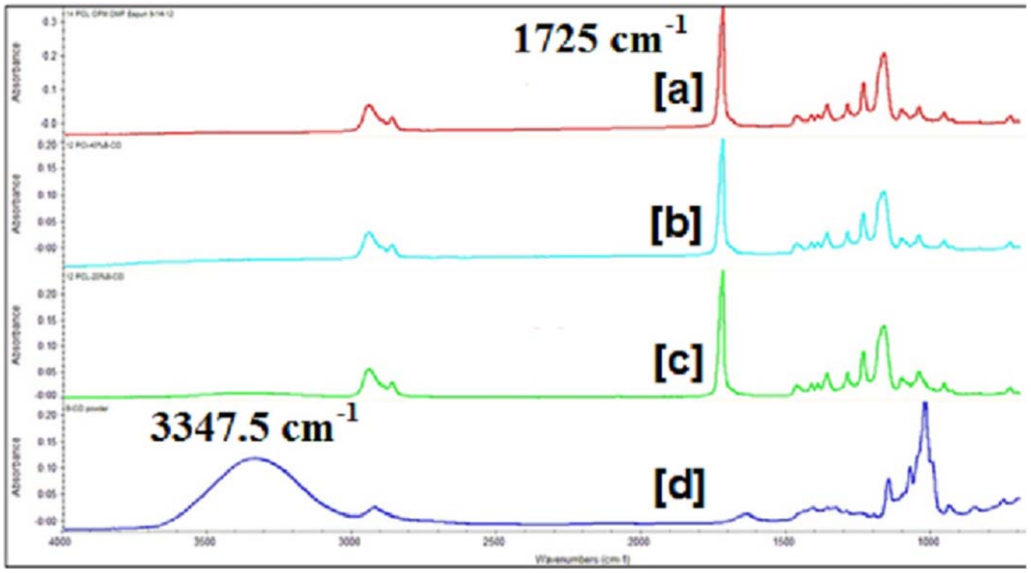

Figure 3. FTIR spectra of electrospun (a) PCL fibers, (b) PCL/40% β-CD, (c) PCL/20% β-CD and (d) neat β-CD powder. [Color figure can be viewed in the online issue, which is available at wileyonlinelibrary.com.]

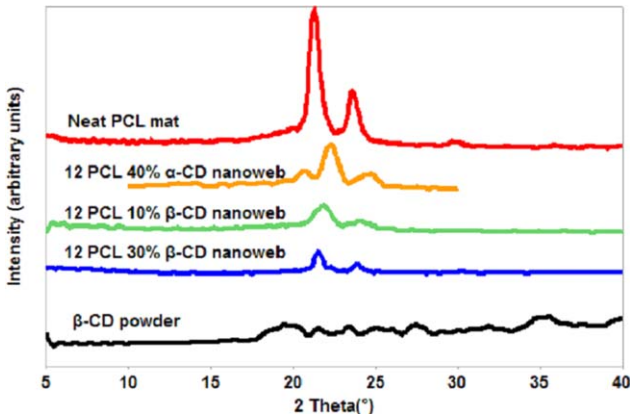

Figure 4. WAXD analysis of (a) neat PCL mat, electrospun nanofibers of (b) PCL/ 40%α-CD (for comparison), (c) PCL/ 10% *β*-CD, (d) PCL/ 30% *β*-CD, and (e) Pure *β*-CD powder. [Color figure can be viewed in the online issue, which is available at wileyonlinelibrary.com.]

observed for the unthreaded PCL chains in our composite nanowebs.[53]TGA results complement the FTIR findings concerning the presence of *β*-CDs, and XRD analyses concerning the presence of a physical mixture in the nanofibers, rather than ICs. Water contact angle provides valuable information about the hydrophilicity/hydrophobicity of the substrate, which plays a crucial role in determining cell-growth if these materials are used as substrates. Representative images and average WCA values of electrospun neat PCL, PCL/20% *β*-CD, and PCL/40% *β*-CD mats after contact of 0 and 30 s are shown in Figure 7.

As expected, neat PCL being a hydrophobic material, exhibited high WCA values (127.3±4.3°). However, upon incorporation of *β*-CDs, a sharp decrease in WCA values was observed for those containing 20% *β*-CD (108.3± 2.5)°. Though statistically significant, those containing 40% *β*-CD elicited only a slightly larger decrease (103.6±1.62)°than those containing 20% *β*-CD. WCA measurements were also conducted after 30s to infer if there is any difference during this time interval. Interestingly, a small decrease was observed for neat PCL, and no significant difference was observed for those containing *β*-CD. A strong reduction in WCA values in *β*-CD containing fibers (~20°)

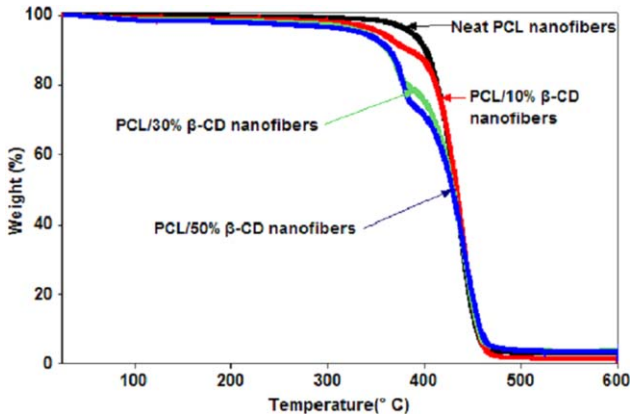

Figure 5. TGA thermograms of neat PCL and functionalized PCL nanofibers from 25°C to 600°C. [Color figure can be viewed in the online issue, which is available at wileyonlinelibrary.com.]

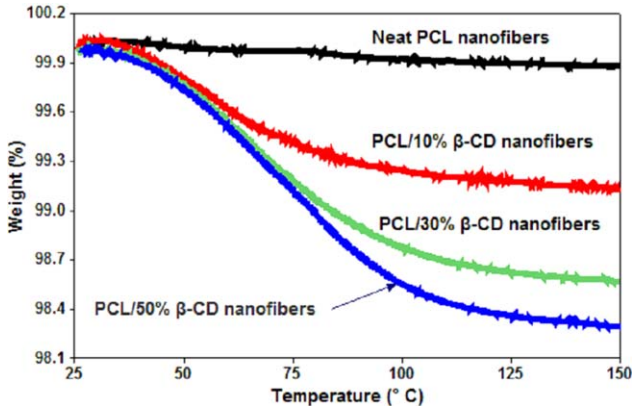

Figure 6. TGA thermograms of neat PCL and functionalized nanofibers from 75°C to 125°C. [Color figure can be viewed in the online issue, which is available at wileyonlinelibrary.com.]

indicate a lesser hydrophobic nature of the functionalized mats, which in turn are expected to result in enhanced cell adhesion and faster wound healing of the skin tissue.

XPS measurements were carried out to characterize the presence of *β*-CDs on the PCL nanofiber surfaces as well as to determine the uptake of butyric and propionic acids by the neat PCL and

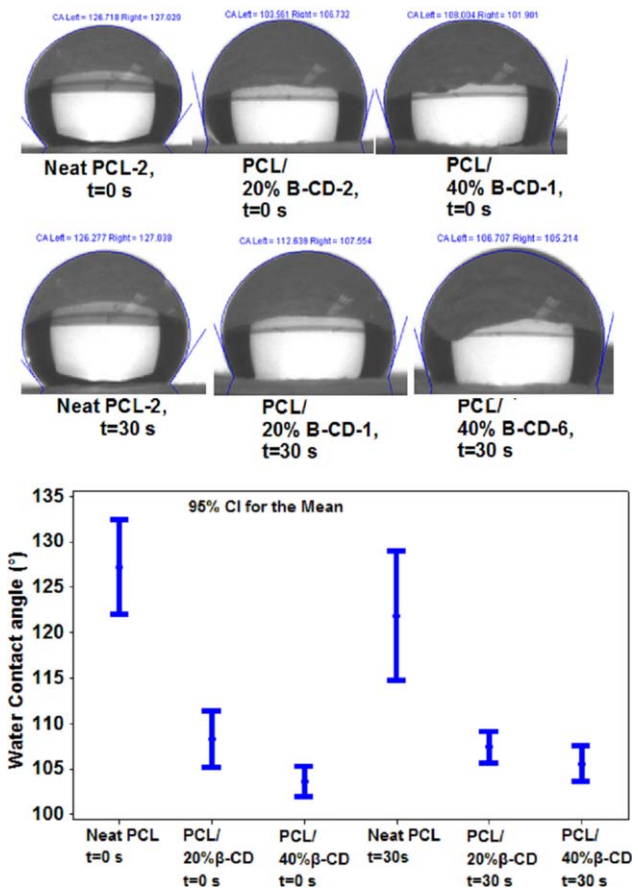

Figure 7. Representative images and water contact angle plots (average of 5 samples) of electrospun neat PCL and PCL/*β*-CD mats. [Color figure can be viewed in the online issue, which is available at wileyonlinelibrary.com.]

Table II. Elemental Composition of PCL and β-CD Functionalized PCL Nanofibers and Corresponding Components of O1s Spectra

Sample	Total carbon content %	Total oxygen content %
Neat PCL	82.47	17.53
PCL/20% β-CD	76.00	24.00
PCL/40% β-CD	73.02	26.98

β-CD functionalized PCL fibers. As mentioned before, with only a halo like hydroxyl peak, FTIR analysis was insufficient to characterize the presence of CDs in the fibers. "Full" spectra of XPS of PCL and β-CD functionalized nanofibers exhibit the presence of C1s and O1s as elements, and their composition is given in Table II. Also, elements such as chlorine and sulfur were not observed, indicating complete removal of potentially toxic solvents (chloroform and DMF) during or after electrospinning (Supporting Information Figures S1–S3).

As expected, with the addition of β-CDs, the % content of oxygen increased considerably (17.5% for neat PCL to 24% for 20% β-CD functionalized PCL nanofibers). Also a % increase of oxygen was observed to be related to the % content of β-CD, *i.e.*, the larger the β-CD content, the higher the % of oxygen (24% for 20% β-CD and 27% for 40% β-CD). This is expected, because β-CD by mass is about 55% oxygen and 45% carbon. Hence, presence of β-CD would inevitably increase the % oxygen content in the physical mixture of PCL and β-CD.

Since there were significant overlaps in the high resolution C1s spectra, O1s spectra, instead were chosen for further wound odor analyses. High resolution O1s spectra of the neat PCL, 20%, and 40% β-CD functionalized nanofibers are shown in Figure 8. O1s spectra of the neat PCL nanofibers indicate two distinct peaks at ~ 531.7 and 533.4 eV, corresponding to C=O*

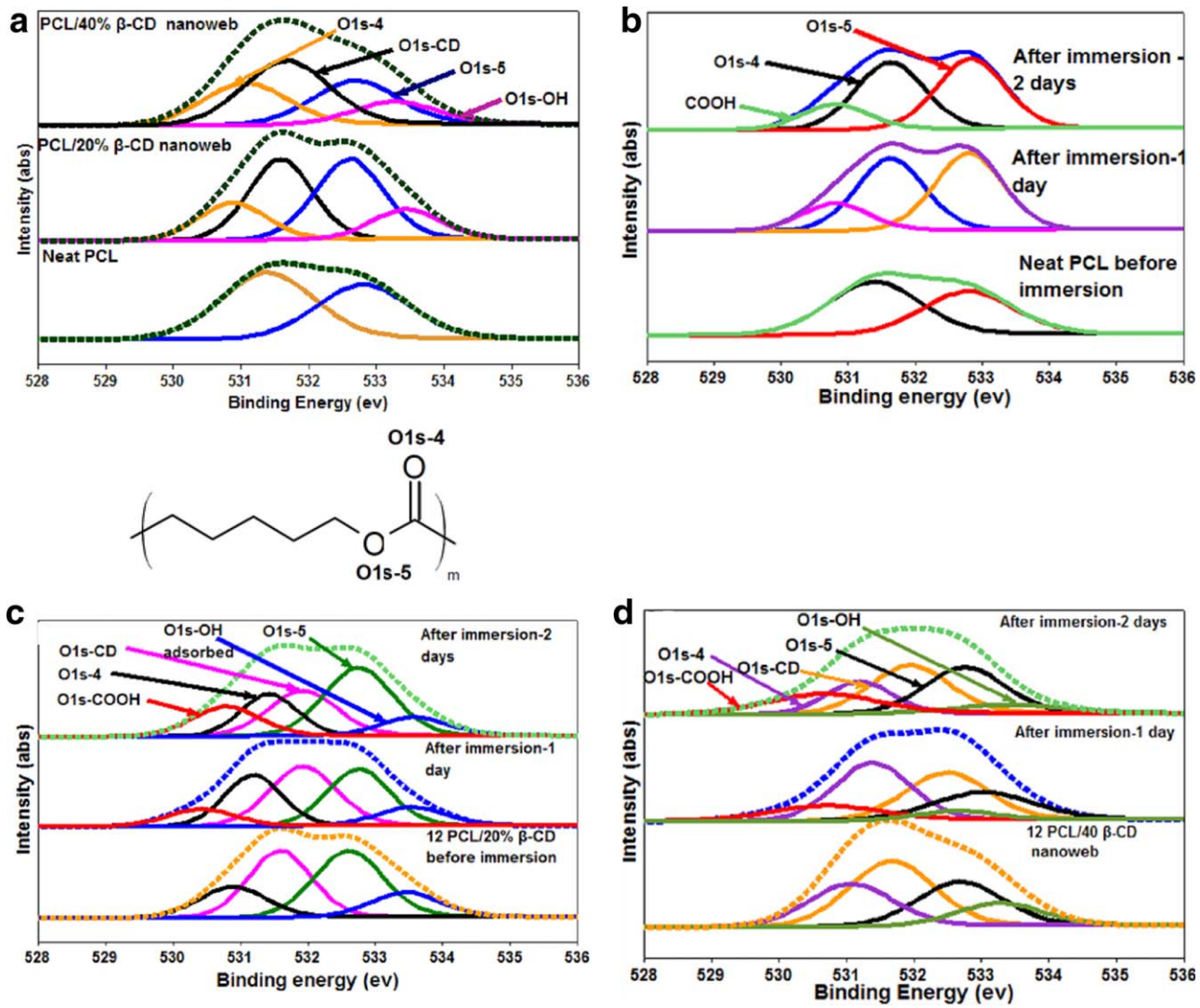

Figure 8. (a) High resolution O1s spectra of PCL and β-CD functionalized PCL nanofibers. (b) High resolution O1s spectra of neat PCL nanofibers before and after immersion tests. (c) High resolution O1s spectra of PCL/20% β-CD nanofibers before and after immersion tests. (d) High resolution O1s spectra of PCL/40% β-CD nanofibers before and after immersion tests. [Color figure can be viewed in the online issue, which is available at wileyonlinelibrary.com.]

and C-O* of the PCL, and their ratio was observed to be 55.47% and 44.43%, respectively. In the case of β-CD functional nanofibers, two new distinct peaks at ~533.15 and 535.2 eV were observed and can be attributed to the hydroxyl groups present in β-CDs (C-O*H) and to the water that is present both within the cavity, as well as those bound on the external hydroxyl groups of the β-CDs. As expected, the % content of hydroxyl groups in the functionalized nanofibers was linearly related to the β-CD content (OH for 40% β-CD> OH for 20% β-CD). However, the water content was observed to be similar for both the functionalized nanofibers (~13%). It is interesting to note that this content is far higher than those reported in the literature.[54] With the addition of β-CDs, decrease in the contents of O1s-4 and O1s-5 was observed, and this phenomenon can simply be attributed to dilution effects. Since XPS is a surface sensitive technique, the presence of two new peaks along with their high content indicates that most of the β-CDs are present on the surface, and hence should possess excellent encapsulation capabilities, as long as their cavities are not occupied. After immersion tests, to determine the efficiency of the nanofibers in absorbing foul acid odors, XPS measurements were carried out, and their obtained O1s spectra are shown in Figure 8(b–d). After immersing the nanowebs in the simulated wound odor fluid, in all the nanofibers, there was an additional peak observed at ~ 530.70 eV. This peak can be attributed to the presence of carboxylic acids.[55] Although unexpected, after 1 day, neat PCL nanowebs had absorbed wound odor and with a estimated to be about 15%.

Interestingly, in the case of PCL/20% β-CD and PCL/40% β-CD nanowebs, the contents of the carboxylic acids were estimated to be only about 10 and 15%, respectively, which is lower than that for neat PCL, especially the 20% β-CD nanowebs. It was also observed that in the case of β-CD functionalized nanofibers, especially for 40% β-CD nanofibers, the water content decreased sharply, indicating inclusion formation with butyric and propionic acids, since the inclusion complexation occurs via expulsion of the water molecules inside the β-CD cavities. After 2 days of immersion, the carboxylic content absorbed by neat PCL nanofibers still remained at about 15%, while those containing β-CDs had increased to 15% and 18% for 20% and 40% β-CD, respectively. A slight decrease in water content was observed in both functional nanofibers, but nevertheless, some water content was still observed, indicating that more room was available for the absorption of foul odors in these functionalized nanofibers.

Two points need to be made here: firstly, the acidic environment typically retards the inclusion formation and, secondly, one of the key driving mechanisms for successful IC formation is the expulsion of high enthalpy water molecules that are present inside the CD cavity.[56] In our case, since only butyric and propionic acids were studied, the acidic environment used possibly decreased the efficiency of IC formation. However, in a real wound exudate, wound odors consist of components such as cadaverine and putrescine, that are alkaline in nature, should tend to neutralize or at the very least increase the pH of the solution. These factors are expected to greatly increase the wound odor uptake by β-CD functionalized PCL nanofibers. Although the neat PCL nanoweb was not expected to absorb butyric and propionic acids, it seemed to. However, during the experiments it was observed that when the neat PCL nanoweb was removed from the solution, there was a strong odor emanating from them, which was not observed with the β-CD functionalized nanofibers. This indicates that the odorants were only very weakly bound to the surfaces of the neat PCL nanowebs. Since XPS measurements were carried out in vacuum, these loosely held compounds were visible in the spectra. Since the objective of this study was to not merely absorb the wound odor chemicals, but to mask them by retention, we can conclude that neat PCL fiber surfaces absorb, but do not retain the odorants, while those containing β-CD both retain and mask the odors, which was further confirmed by TGA (discussed later).

In the case of β-CD functionalized nanofibers, after two days of immersion, it was observed that the water content was about 8% and 9%, for 20% β-CD and 40% β-CD, respectively. These high water content values indicate, in both cases, at least half of the β-CDs are in the uncomplexed form, and which are expected to form ICs with wound odor molecules if provided sufficient time. This result was supported by GC data, where it was observed that the saturation point of uptake of the wound odor molecules was observed to occur somewhere around 4 days (Supporting information S4 and S5).

TGA measurements were carried out on the nanowebs before and after the immersion tests to investigate the thermal stability of the nanofibers, which should also indicate the presence of the acids. TGA thermograms of neat PCL nanoweb, 20% β-CD, and 40% β-CD functionalized fibers before and after immersion are shown in Figure 9(a–c), respectively. Thermal degradation of neat PCL nanowebs before immersion indicates, a single degradation pattern that starts at about 380°C, and increases rapidly around 410°C, at which point the complete destruction of PCL takes place, as reported in the literature.[35] In the case of the neat PCL nanoweb, after 1 and 2 days immersion experiments, both elicit a strikingly similar degradation pattern. Although, thermal degradation of butyric or propionic acids could not be obtained from the literature, mass loss because of dehydration at 100°C, and degradation of carboxylic acid structures are expected. But in the thermograms of neat PCL, there was no dehydration noted or any mass loss observed between 30°C and 400°C. The absence of these two patterns indicates the absence of any retained wound odor compounds.

However, in the case of β-CD functionalized PCL nanofibers, in addition to the thermal degradation of PCL at ~410°C, two more recognizable degradation steps take place. Firstly, there is a water weight loss at about 100°C, and secondly, there is thermal degradation of β-CDs, which starts at about 320°C and proceeds till about 370°C. Further, the water loss observed for the functionalized nanofibers depended on the % β-CD content (Figures 5 and6). The thermal degradation of β-CD is typically seen as a "slanted broad U" pattern (highlighted in the thermogram) that starts at about 320°C and ends with the commencement of PCL degradation. The broadness of the "slanted U" pattern depends on the added % β-CD content, *i.e.,* the higher the β-CD content, the broader is the pattern. When the β-CD forms an inclusion compound with a small guest molecule,

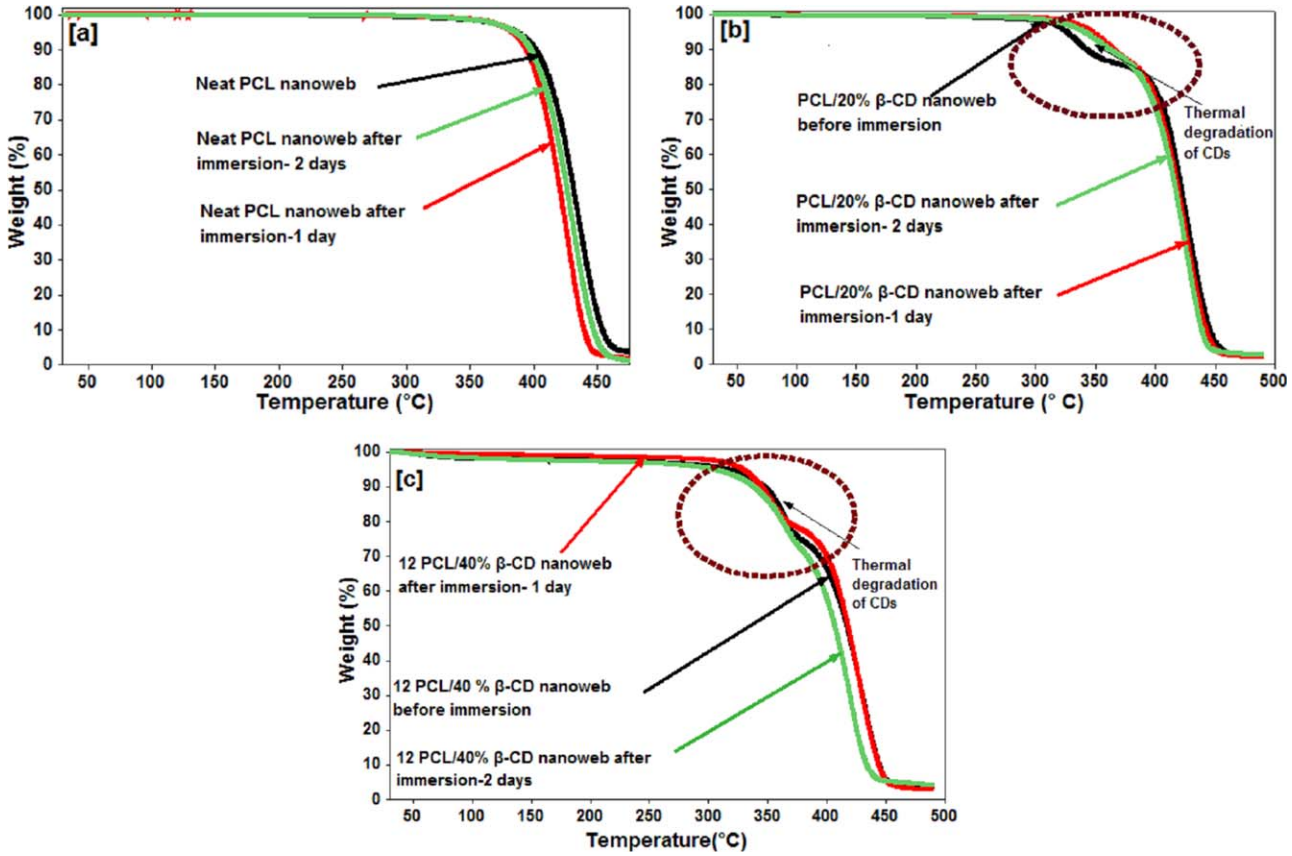

Figure 9. (a) TGA thermograms of nanowebs before and after immersion in wound odor solution. Neat PCL nanowebs. (b) TGA thermograms of nanowebs before and after immersion in wound odor solution. 20% β-CD functionalized PCL nanowebs. (c) TGA thermograms of nanowebs before and after immersion in wound odor solution. 40% β-CD functionalized PCL nanowebs. [Color figure can be viewed in the online issue, which is available at wileyonlinelibrary.com.]

however, the degradation pattern significantly changed; depending on the degree of IC formation, the "slanted U pattern" straightens out.

From the thermograms of the functionalized nanofibers, it is clear that after immersion tests; the "slanted broad U" like pattern "straightens" progressively (highlighted in the thermograms [Figure 9(b,c)]. A marked decrease in the CD degradation pattern is observed for both the nanowebs at even 1 day, and a further drastic change is observed at 2 days. It is also clear from the thermograms [Figure 9(b,c)] that the "slanted U like pattern" did not disappear completely, meaning, there is further room for IC formation with the acids. These results support the XPS data that show neat PCL nanofibers do not mask any odor, while β-CD functionalized PCL nanofibers do.

As mentioned before, this study was conducted as a proof of concept to examine the possibility of utilizing β-CD functionalized PCL nanofibers for removing wound odor. Since the functional nanofibers possess β-CD in the form of cage structures, slightly longer chain fatty acids such as valeric acid, which typically is a wound odor compound, can only form ICs with columnar CDs.[57] Observations reported[58–61] for formation of CD-ICs using solid host cage CDs and guests that complex only in columnar ICs demonstrate that if the host CD is used in its solid columnar form the columnar IC will be formed much faster than beginning with cage CDs. Hence, novel ways to electrospin β-CDs that results in a channel type structure should be investigated, as it can potentially facilitate absorption of such acids. For simplicity, only two short chain fatty acids, viz. butyric and propionic acids, were investigated in this study. A full factorial design experiment consisting of a simulated wound fluid needs to be conducted. The model fluid used could be such that it replicates wound fluids typically observed in diabetic patients.

Aqueous solutions were not considered in our experiments, since the presence of water might potentially dissolve or leach out the β-CDs. However, recently, Uyar *et al.* reported the formation of cross-linked electrospun polyester/β-CD moieties, using citric acid as cross linker.[46] From a biomedical standpoint, use of citric acid as cross linker might not be desirable, as it is acidic, and might hinder cell growth, as is typically observed for acrylic acid-grafted polymeric systems.[49] Other option such as using glutaraldehyde for cross-linking might also not be desirable because of toxicity considerations.

Ultra-violet (UV) induced crosslinking offers an environmentally benign, biomedically friendly alternative route to solve this issue. Recently, polydimethyl siloxane was reported to be cross-linked using UV with benzophenone as catalyst.[62] Since PCL has methylene groups, it could be feasible to UV crosslink a

PCL-CD composite. Moreover, since benzophenone melts at less than 47°C, PCL/β-CD webs could be melt processed without the destruction of nanofibrous structure, and subsequently UV crosslinked.

CONCLUSIONS

β-CD functionalized composite nanofibers containing PCL and β-CDs were prepared using an electrospinning process. Presence of β-CDs in the mats was verified using FTIR, XPS, and by water loss through TGA. Average fiber diameter of a neat PCL control web was found to be around 400 nm, while that of the composite web fibers containing β-CD were found to be about 500 nm.

Unlike α- and γ-CD functionalized PCL nanofibers reported in our previous study.[40] TGA observations indicate the degradation patterns of β-CD functionalized materials to be a simple mixture, rather than ICs. This result was further confirmed by the absence of IC peaks in the XRD analysis. By virtue of an increase in the % oxygen content, XPS analyses indicated, significant presence of β-CDs on the composite nanoweb surfaces. Similar to α- and γ-CD functionalized PCL nanofibers, water contact angle measurements indicated that with addition of β-CDs, there is a sharp decrease in WCA values.

The absorption of wound odor solution consisting of butyric and propionic acids by neat and functionalized PCL nanofibers was examined using XPS. Although, the XPS indicated the presence of the acids in the neat PCL mats, TGA conclusively indicated absence of any such moieties. This was a result of the inability of the neat PCL nanoweb to hold/retain the carboxylic acid odorants after drying. On the other hand, functionalized nanofibers, especially, those containing 40% β-CD, absorbed and retained much higher amounts of odor compounds, with the possibility of taking up even more, if provided more time. As we demonstrated, higher loadings of β-CDs are possible, which would also help increase the uptake of these odors.

It would be desirable to study the absorption of simulated wound fluids containing all components, such as both the amines and the short chain fatty acids, using XPS, TGA and even more advanced technologies, such as the electronic nose (e-nose). From our observations of short chain fatty acids, in a real wound fluid of neutral or at least at a higher pH, we would expect β-CD functionalized PCL nanofibers to perform even better.

ACKNOWLEDGMENTS

The authors acknowledge the use of the Analytical Instrumentation Facility (AIF) at North Carolina State University, which is supported by the State of North Carolina and the National Science Foundation, and in particular Fred Stevie and Elaine Zhou, of AIF, for XPS data analyses.

REFERENCES

1. Kim, B.-S.; Kim, I.-S. *Polym. Rev.* **2011**, *51*, 235.
2. Frenot, A.; Chronakis, I. S. *Curr. Opin. Colloid Interface Sci.* **2003**, *8*, 64.
3. Tong, H.-W.; Wang, M. *J. Macromol. Sci., Part B: Phys.* **2011**, *50*, 1535.
4. Bhardwaj, N.; Kundu, S. C. *Biotechnol. Adv.* **2010**, *28*, 325.
5. Jin, L.; Wang, T.; Zhu, M.-L.; Leach, M. K.; Naim, Y. I.; Corey, J. M.; Feng, Z.-Q.; Jiang, Q. *J. Biomed. Nanotechnol.* **2012**, *8*, 1.
6. McCann, J. T.; Li, D.; Xia, Y. *J. Mater. Chem.* **2005**, *15*, 735.
7. Mehraban, M.; Zadhoush, A.; Ravandi, S. A. H.; Bagheri, R.; Tehrani, A. H. *J. Appl. Polym. Sci.* **2013**, *128*, 926.
8. Finne-Wistrand, A.; Albertsson, A.Cl.; Kwon, O. H.; Chen, G.; Kang, K.; Hasuda, H.; Gong, J.; Ito, Y. *Macromol. Biosci.* **2008**, *8*, 951.
9. Moghe, A. K.; Hufenus, R.; Hudson, S. M.; Gupta, B. S. *Polymer* **2009**, 3311.
10. Celebioglu, A.; Uyar, T. *Mater. Lett.* **2011**, *65*, 2291.
11. Lee, B. N.; Kim, D. Y.; Kwon, J. S.; Park,Y. H.; Chun, H. J.; Kim, J. H.; Lee, H. B.; Min, B. H.; Kim,M. S. *J. Biomed. Mater. Res. A* **2012**, *100*, 1751.
12. Moura, L. I. F.; Dias, A. M. A.; Carvalho, E.; De Sousa, H. C. *Acta Biomater.* **2013**, *9*, 7013.
13. da Silva, L.; Carvalho, E.; Cruz, M. T. *Expert Opin. Biol. Ther.* **2010**, *10*, 1427.
14. Enoch, S.; Leaper, D. J. *Surgery* **2008**, *26*, 31.
15. Fromantin, I.; Seyer, D.; Watson, S.; Rollot, F.; Elard, J.; Escande, C.; De Rycke, Y.; Kriegel, I.; Garde, V. L. *J. Clin. Microbiol.* **2013**, *51*, 3368.
16. Leveen, H. H.; Falk, G.; Borek, B.; Diaz, C.; Lynfield, Y.; Wynkoop, B. J.; Mabunda, G. A.; Rubricius, J. L.; Christoudias, G. C. *Ann. Surg.* **1973**, *178*, 745.
17. Rodriguez, P. G.; Felix, F. N.; Woodley, D. T.; Shim, E. K. *Dermatol. Surg.* **2008**, *34*, 1159.
18. Bradley, M.; Cullum, N.; Nelson, E. A; Petticrew, M.; Sheldon, T.; Torgerson, D. *Health Technol. Assess.* **1999**, *3*, 1.
19. Winter, G. D. *Nature* **1962**, *193*, 293.
20. Lloyd, L. L.; Kennedy, J. K.; Methacanon, P.; Paterson, M.; Knill, C. J. *Carbohydr. Polym.* **1998**, *37*, 315.
21. Fonder, M. A.; Lazarus, G. S.; Cowan, D. A.; Aronson-Cook, B.; Kohli, A. R.; Mamelak, A. J. *J. Am. Acad. Dermatol.* **2008**, *58*, 185.
22. Skorkowska-Telichowska, K.; Czemplik, M.; Kulma, A.; Szopa, J. *J. Am. Acad. Dermatol.* **2011**, *5*, 1.
23. Hilton, J. R.; Williams, D. T.; Beuker, B.; Miller, D. R.; Harding, K. G. *Clin. Infect. Dis.* **2004**, *39*, 100.
24. Lipman, R. D. A.; van Bavel, D. Odor absorbing hydrocolloid dressings for direct woundcontact. *Wounds Res.* **2007**.
25. Exuderm® Odorshield™. Wound dressing, the first odor-control hydropolymer, Medline. Available at: http://www.medline.com/jump/product/x/Z05-PF00173. (accessed April 15, **2015**).
26. Szejtli, J. In Cyclodextrin Technology; J. E. D. Davies, Ed., Kluwer Academic Publishers: Boston, MA, **1988**; p 1.
27. Kayacki, F.; Uyar, T. *Food Chem.* **2012**, *133*, 641.
28. Tonelli, A. E. *Adv. Polym. Sci.* **2009**, *222*, 115.

29. Huang, L.; Tonelli, A. E. *J. Macromol. Sci. Part C: Polym. Rev.* **1998**, *38*, 781.
30. Huang, L.; Gerber, M.; Lu, J.; Tonelli, A. E. *Polym. Degrad. Stab.* **2001**, *71*, 279.
31. Huang, L.; Taylor, H.; Gerber, M.; Orndorff, P. E.; Horton, J. R.; Tonelli, A. E. *J. Appl. Polym. Sci.* **1999**, *74*, 937.
32. Whang, H. S.; Hunt, M. A.; Wrench, N.; Hockney, J. E.; Farin, C. E.; Tonelli, A. E. *J. Appl. Polym. Sci.* **2007**, *106*, 4104.
33. Szente, L.; Szejtli, J. *Trends Food Sci. Technol.* **2004**, *15*, 137.
34. Tonelli, A. E. *Beilstein J. Org. Chem.* **2012**, *8*, 1318.
35. Uyar, T.; Havelund, R.; Nur, Y.; Balan, A.; Hacaloglu, J.; Toppare, L.; Basenbacher, F.; Kingshott, P. *J. Membr. Sci.* **2010**, *365*, 409.
36. Uyar, T.; Havelund, R.; Hacaloglu, J.; Kingshott, P. *ACS Nano* **2010**, *4*, 5121.
37. Kayaci, F.; Umu, O. C. O.; Tekinay, T.; Uyar, T. J. *Agric. Food Chem.* **2013**, *61*, 901.
38. Kayaci, F.; Aytac, Z.; Uyar, T. *J. Agri. Food Chem.* **2013**, *61*, 8156.
39. Fatih Canbolat, M.; Celebioglu, A.; Uyar, T. *Colloids Surf. B* **2014**, *116*, 612.
40. Narayanan, G.; Gupta, B. S.; Tonelli, A. E. *Biomacromolecules* **2014**, *15*, 4122.
41. Huang, L.; Allen, E.; Tonelli, A. E. *Polymer* **1998**, *39*, 4857.
42. Rusa, C. C.; Fox, J.; Tonelli, A. E. *Macromolecules* **2003**, *36*, 2742.
43. Shuai, X.; Porbeni, F. E.; Wei, M.; Bullions, T.; Tonelli, A. E. *Macromolecules* **2002**, *35*, 2401.
44. Williamson, B. R.; Tonelli, A. E. *J Inclusion Phenom. Macrocyclic Chem.* **2012**, *72*, 71.
45. Chan, S.-C.; Kup, S.-W.; Chang, F.-C. *Macromolecules* **2005**, *38*, 3099.
46. Kayaci, F.; Aytac, Z.; Uyar, T. *J. Hazard. Mater.* **2013**, *261*, 286.
47. Stalder, A. F.; Melchior, T.; Müller, M.; Sage, D.; Blu, T.; Unser, M. *Colloids Surf. A* **2010**, *364*, 72.
48. Uyar, T.; Havelund, R.; Hacaloglu, J.; Zhou, X.; Besenbacher, F.; Kingshott, P. *Nanotechnology* **2009**, *20*, 125605.
49. Gupta, B.; Plummer, C.; Bisson, I.; Frey, P.; Hilborn, J. *Biomaterials* **2002**, *23*, 863.
50. Gao, J.; Yu, S.; Zheng, B.; Song, Q.; Peng, X.; Lin, Y.; Zou, G.; Zhang, Q. *RSC Adv.* **2014**, *4*, 36675.
51. Jia,Y.-T.; Gong, J.; Gu, X.-H.; Kim, H.-Y.; Dong, J.; Shen, X.-Y. *Carbohydr. Polym.* **2007**, *67*, 403.
52. Uyar, T.; Rusa, C. C.; Hunt, M. A.; Aslan, E.; Hacaloglu, J.; Tonelli, A. E. *Polymer* **2005**, *46*, 4762.
53. Porbeni, F. E.; Edeki, E. M.; Shin, I. D.; Tonelli, A. E. *Polymer* **2001**, *16*, 6907.
54. Kayaci, F.; Uyar, T. *Polym. Eng. Sci.* **2014**, *54*, 2970.
55. Yatsimirskii, K. B.; Nemoskalenko, V. V.; Aleshin, V. G.; Bratushko, Y. I.; Moiseenoo, E. I. *Chem. Phys. Lett.* **1997**, *52*, 481.
56. Yu, J.-S.; Wei, F.-D.; Zhao, C. *Spectrochim. Acta Part A* **2002**, *58*, 249.
57. Huang, L.; Tonelli, A. E. *Polymer* **1999**, *40*, 3211.
58. Rusa, M.; Wang, X.; Tonelli, A. E. *Macromolecules* **2004**, *37*, 6898.
59. Peet,J.; Rusa, C. C.; Hunt, M. A.; Tonelli, A. E.; Balik, C. M. *Macromolecules* **2005**, *38*, 537.
60. Harada, A.; Okada, M.; Kawaguchi, Y. *Chem. Lett.* **2005**, *34*, 542.
61. Hunt, M. A; Tonelli, A. E.; Balik, C. M. *Polymer* **2008**, *49*, 985.
62. Bhagat, A. A. S.; Jothimuthu, P.; Paputsky, I. *Lab Chip* **2007**, *7*, 1192.